processes

MDPI

Article

Upgrading Waste Activated Carbon by Equipping Micro-/Mesopore-Dominant Microstructures from the Perspective of Circular Economy

Tsing-Hai Wang [1,*], Chun-Chi Chen [1], Ruo-Xin Xu [1], Chiu-Wen Chen [2] and Cheng-Di Dong [2]

[1] Department of Chemical Engineering and Materials Science, Yuan Ze University, Taoyuan 320, Taiwan
[2] Department of Marine Environmental Engineering, National Kaohsiung University of Science and Technology, Kaohsiung 811, Taiwan
* Correspondence: thwang@saturn.yzu.edu.tw

Abstract: Equipping wastes with interesting properties in response to the circular economy could release environmental burdens by reducing resource exploitation and material manufacturing. In this study, we demonstrated that the waste regenerated activated carbon (RAC) could become micro-/mesopore-dominant through a simple surfactant/gel modification. This was achieved by associating carbon precursors, such as commercially available low-cost surfactants/methyl cellulose thickening reagents, with the pores of RAC. Following heat treatment, associated carbon precursors were carbonized, hence modifying the microstructure of RAC to be micro-/mesopore-dominant. The surfactant modification gave rise to a micropore-dominant RAC by increasing the micropore volume (PV_{micro}) together with significantly decreasing the mesopore volume (PV_{meso}) and macropore volume (PV_{macro}). In contrast, gel modification led to mesopore-rich RAC by blocking micropores with carbonized methyl cellulose and a surfactant matrix. Interestingly, both surfactant/gel modifications were insensitive to the properties of the surfactant applied, which provided a new alternative for waste/low-grade surfactant mixture disposal. Our results provide an important demonstration that waste could be effectively upgraded with a rational design by exhibiting new properties in response to the circular economy.

Keywords: activated carbon; circular economy; microstructure; surfactants

Citation: Wang, T.-H.; Chen, C.-C.; Xu, R.-X.; Chen, C.-W.; Dong, C.-D. Upgrading Waste Activated Carbon by Equipping Micro-/Mesopore-Dominant Microstructures from the Perspective of Circular Economy. *Processes* **2022**, *10*, 1631. https://doi.org/10.3390/pr10081631

Academic Editor: Chung-Yu Guan

Received: 31 July 2022
Accepted: 16 August 2022
Published: 17 August 2022

1. Introduction

Activated carbon (AC) is a carbonaceous material with a high surface area arising from its porous structure and has been frequently used for purification and separation [1]. The high surface area allows AC to serve as an appropriate support to disperse catalysts effectively [2]. AC also functions as an effective reductant, such as for preparing silver nanoparticles for carbon paste electrode application [3]. In light of electrochemical applications, such as supercapacitors, a hierarchical porous structure is another important feature in addition to the high surface area. This is because the selectivity is strongly related to the dehydration penalty that thermodynamically regulates the accessibility of an ion approaching the pores [4]. Furthermore, the short channel length due to the large pore size significantly enhances the performance of supercapacitors [5]. A carbonaceous material with a narrow pore size distribution, high surface area, and large pore volume is highly valuable. The utilization of a template is a reliable synthesis route to obtain a carbonaceous material with a narrow pore size distribution. For example, controlled high-temperature pyrolysis of polyimide produces subsequent carbon molecular sieve disordered turbostratic structures with plates resulting from the aromatized strands and micropores by voids between the plates [6]. The high-temperature pyrolysis of ion-exchange resin under a CO_2 atmosphere produced AC with a high mesopore fraction [7]. Additional chemical activation yielded hierarchical porous carbon with a micropore-rich structure [6,7].

Recently, increased awareness of the circular economy has driven a movement to upgrade produced waste. Waste utilization to prepare hierarchical porous carbon has accordingly attracted intense research interest. Cellulose-rich biomass, such as garlic seeds [8] and corncobs [9], is a promising renewable carbon source to prepare porous AC with a high surface area. Carbonization followed by the activation of crosslinked lignosulfonate in waste pulp mills with glutaraldehyde and ethyleneimine polymer has yielded large-surface-area AC with pore sizes of <4 nm [10]. In these successful demonstrations, chemical activation agents, such as $ZnCl_2$ [11] and KOH [12], were required. However, an additional acid wash to remove the residual activating agents is necessary. The cost of the activating agent and the waste acid effluent treatment would be an issue of concern. Hence, we consider whether waste AC that has already been equipped with a large surface area would be an alternative starting material to prepare hierarchical porous carbon. In addition to avoiding the usage of chemical activation reagents, the significance of the proposed concept is that it can upgrade waste ACs by decorating them with a new hierarchical microstructure from the perspective of the circular economy. The upgrade is achieved by dispersing carbon precursors, such as commercially available low-cost surfactants and methyl cellulose thickening agents, in the pores of waste AC [13]. The carbonization of associated carbon precursors in the following heat treatment would repartition the microstructure of the regenerated AC (RAC) to be either microporous or meso-/macroporous (Figure 1). Furthermore, the as-obtained RAC could be upgraded by exhibiting a new microstructure that extends its applications. Our result would provide an important demonstration that arranging an appropriate treatment route could upgrade the produced wastes by giving them new surface properties based on the circular economy consideration.

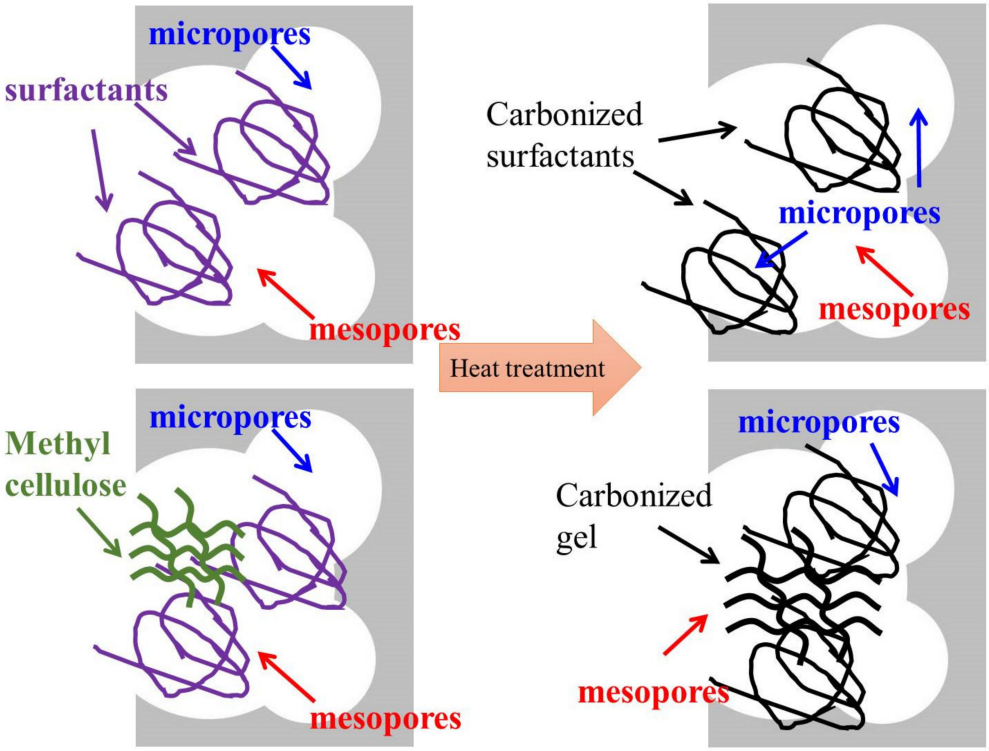

Figure 1. Illustration of upgrading through microstructure manipulation by the carbonization of carbon precursors in pores of waste AC.

2. Experimental

2.1. Chemicals and Preparation of Surfactant/Gel Modified RAC

Coal-based cylinder-regenerated AC (referred to as AC ref) was provided by China Activated Carbon Industries LTD (CACI), Guanyin, Taiwan, and used as received. As the

mechanical strength of these RACs failed the quality control by the company, they would be directly disposed of; therefore, they are an appropriate model material. Eight commercially available low-cost surfactants (First Chemical, Taiwan) (Table 1) [14] were selected to reduce the concern associated with the operation cost. To synthesize surfactant/gel-modified RAC, 5 g of AC ref was dispersed in 500 mL surfactant/gel solutions for 24 h. The surfactant solutions contained 5 mL of the selected surfactant and 495 mL of deionized water. The obtained RAC was hence referred to as, for example, surf 1, indicating that the sample was modified using surfactant 1. The gel solutions were prepared by mixing 5 mL of the selected surfactant and 0.5 g methyl cellulose thickening agent (First Chemical, Taipei, Taiwan) in 495 mL of deionized water. Similarly, the gel-modified RAC was described as, for example, gel 1, indicating that it was modified in the gel containing surfactant 1. The AC samples were separated from the surfactant/gel solution, dried at 60 °C for 24 h, subjected to 600 °C thermal treatment in a tube furnace (heat ramp of 10 °C/min and 4 h hold time), and then cooled down to room temperature under N_2 flow (flow rate of 150 cm^3 min^{-1}). The adopted mild thermal treatment process was identical to the regeneration protocol of CACI to reduce the operation cost, even though high-temperature activation is known to yield high surface area effectively [15]. The AC ref was also dispersed in 500 mL of deionized water and subjected to the identical regeneration process for comparison.

Table 1. Properties of the selected surfactants used in this study.

Abbr.	Chemical Structure	CAS No.	Content (%)	Molecular Formula	Description	CMC [a] (mM)
1	Potassium cocoyl glycinate	301341-58-2	28	$C_{13}H_{27}CONHCH_2COOK$	Anionic	0.21
2	Sodium lauroyl sarcosinate	137-16-6	30	$C_{11}H_{23}CONCH_3CH_2COONa$	Anionic	14.57
3	Sodium lauryl ether sulfate	68585-34-2	70	$C_{12}H_{26}O(C_2H_4O)_2SO_3Na$	Anionic	0.80
4	Alcohols, C12–14, ethoxylated, sulfates, and sodium salts	68891-38-3	28	$C_{12}H_{23}(C_2H_4O)SO_4Na$	Anionic	0.14
5	Triethanolamine lauryl sulfate	139-96-8	40	$C_{12}H_{25}SO_4H{\cdot}N(C_2H_5OH)_3$	Anionic	5.91
6	Poly(ethylene glycol) (12) tridecyl ether	78330-21-9	99	$C_{13}H_{27}(C_2H_4O)_{12}OH$	Nonionic	0.15
7	Polyoxyethylene(23) lauryl ether	9002-92-0	88	$C_{12}H_{25}(C_2H_4O)_{23}OH$	Nonionic	0.09
8	Octylphenol ethoxylates (Triton X-305)	9002-93-1	70	$C_{14}H_{22}(C_2H_4O)_{30}OH$	Nonionic	0.24

Note: [a] the critical micelle concentration (CMC) was adopted from Mukerjee and Mysels, 1971 [14].

2.2. Characterization

The surface morphology of the raw/modified RAC was analyzed using field-emission scanning electron microscopy (FESEM, JSM-6701F, JEOL, Tokyo, Japan) equipped with an energy dispersive X-ray (EDX) (Oxford Instruments, Cambridge, UK). The SEM specimens were prepared by adhering RAC to copper tape and depositing a conductive platinum overlayer. X-ray fluorescence (XRF) was used to evaluate the mineral contents in raw/modified RAC (S8 TIGER, Bruker, AXS GmbH, Karlsruhe, Germany). XRF specimens were prepared by mixing 0.5 g of raw/modified RAC with 3.0 g of wax powder and hydraulically pressing into 8 mm diameter cylinders. Identical specimens were also used in X-ray diffraction (XRD) analysis (Cu Kα = 1.5406 Å, D2 Phaser, Bruker, AXS GmbH, Karlsruhe, Germany). The FTIR spectra of the raw/modified RAC were obtained with a Vertex80v, Bruker FTIR (Bruker, AXS GmbH, Karlsruhe, Germany) operated in the single-spot ATR reflectance mode, with a KBr beam splitter, DTGS detector, 4 cm^{-1} resolution, and 200 scans. The size of the surfactant micelles was estimated using dynamic light scattering measurement (DLS, NanoPlus-3, Particulate Systems, Norcross, GA, USA) with the diluted (10×) surfactant solutions used for the modification. Microstructure analysis was conducted by the physisorption of N_2 at 77 K (ASAP 2020, Micromeritics Instrument Corporation, Norcross, GA, USA) with samples previously degasified for 6 h at 90 °C with10 μm Hg. The specific surface area reported herein was the BET surface area. The micropore volume (PV_{micro}) was determined using the t-Plot micropore volume. In contrast, the pore volume of the mesopores (PV_{meso}) and macropores (PV_{macro}) was obtained by the BJH desorption cumulative volume of pores between 17 Å and 3000 Å diameters [16]. The BET method was inevitably short in separating the processes of mono-multilayer adsorption from micropore filling and condensation at pores <4 nm [16]. As no single experimental technique could accurately evaluate the absolute microstructure properties, all values reported herein were

consistently adopted from the physisorption of N_2 at 77 K, as suggested by the ISO standard method [16]. Accordingly, in some cases, the reported total pore volume (PV_{tot}) might not be precisely equal to the sum of PV_{micro} and $PV_{meso} + PV_{macro}$. This is because PV_{tot} was derived from the single point adsorption, while PV_{micro} was determined from the t-Plot and $PV_{meso} + PV_{macro}$ was calculated from the BJH desorption cumulative volume of pores. The quality control of microstructure analysis was conducted by averaging the experimental data of the samples obtained from three different synthesis batches (n = 3). The reported values were the average value with standard deviations. The curves of the microstructure properties, such as the pore size distribution and cumulative pore volume, were adopted from the one that exhibited the surface area closest to the average value. The electrochemical behaviors of the modified RAC were analyzed using a CHI electrochemical station (6081E, CHI Instrument, Austin, TX, USA).

3. Results and Discussion

3.1. Characterization of RAC

Representative XRD patterns of the raw AC (AC ref) and surfactant-modified RAC are shown in Figure S1a. AC ref exhibited a broad diffraction peak at 2θ = 10°–30°, which was attributed to the amorphous carbon composed of aromatic carbon sheets oriented in a considerably random fashion [17]. An appreciable diffraction peak at 2θ = 35°–50° of AC ref was assigned to the axis of the graphite structure [17]. This indicates that the used AC ref was a mixture of amorphous carbon and graphite. Surf 1 (the RAC modified using surfactant 1) possessed an almost identical XRD pattern to AC ref. This means that the characteristics of the mixture of amorphous carbon and graphite were well retained upon the 600 °C 4 h regeneration process. Without effective catalysts, graphitization occurs only at high temperatures (>800 °C) [18], as it involves the polycondensation of existing aromatic layers and the formation of new aromatic layers [19]. An Fe/Mn-based catalyst can effectively improve the graphitization of carbon nanotubes [20]. The combination of calcium chloride and potassium oxalate has recently been acknowledged as a green activator to regulate graphitization [21]. This was achieved by the in situ formation of the $K_2CO_3/CaCO_3$ double-carbonate system, in which the former functioned as the activating agent, while the latter behaved as hard templates [22]. The mineral contents were low (the results of XRF analysis indicated that the Fe, Mn, K, Na, and Ca contents in the ref AC were <2 wt%). Thus, the mild treatment temperature was responsible for the unnoticeable changes in the degree of graphitization of the RAC and surf samples. Representative FTIR spectra of the raw/surfactant-modified RAC and the used surfactants are shown in Figure S1b. It should be noted that, although surfactant 1, the anionic potassium cocoyl glycinate, and surfactant 6, the nonionic poly (ethylene glycol) (12) tridecyl ether, had different chemical structures (Table 1) [14], their FTIR spectra highly resembled those of each other. They both possessed characteristic peaks centered at 1040, 1460, 1680, 2930, and 3460 cm^{-1} corresponding to the C–C deformation, $–CH_2$, C=O, $–CH_3$, and N-H/O-H functional groups [23]. The observed interference fringes at ~1460 cm^{-1} likely originated from the multiple reflections of light within the film-like sample. The spectra were collected by dipping into liquid surfactants at the ATR reflectance module under continuous N_2 flow. The moisture would gradually evaporate under this configuration, leaving the film-like surfactant sample for the FTIR measurement. Unfortunately, although we expected that the modification would introduce new functionality [24,25], no appreciable functional groups could be found in the obtained FTIR spectra. The descended baselines of the raw (AC ref), surf 1, and surf 6 samples from the high-wavenumber region to the low-wavenumber end (Figure S1b) were attributed to the carbonaceous material having deeper light penetration at the low-wavenumber end. The descending baseline further complicated the assignment of functional groups introduced by the modification. Considering that the objective of this study is to upgrade the RAC by manipulating its microstructure, we focus on the changes in microstructure as a result of modification.

The micelle size of a surfactant is an interesting property as it significantly influences the pore size of the synthesized material [25,26]. The means of dynamic light scattering (DLS) were hence adopted to measure the micelle size of eight surfactants (Figure S2a). It must be mentioned in advance that, in the 1 min DLS measurement, the peaks' intensities and locations changed dynamically, particularly those centered at > 100 nm. As the loadings of the eight surfactants far exceeded their critical micelle concentrations (CMC) (Table 1) [14], the intense peak centered at 2 nm suggested that the micelle size of surfactant 1 would be about 2 nm. Two minor peaks around 200–500 nm that sometimes disappeared during DLS measurement likely resulted from the micelle aggregates. Interestingly, despite the different chemical structures between the selected surfactants (Table 1), their dynamic micelle sizes were relatively consistent, lying around 2–3 nm (these results are not presented as they are almost identical). Based on our DLS analysis, the surfactant aggregates/micelles would likely reside in the mesopore. Following the carbonization of the surfactant aggregates/micelles, mesopores transformed into several micropores, yielding a microporous RAC. Representative SEM images of the surf 1 sample are shown in Figure S2b (200×) and Figure S2c (2000×). Visible pores due to stacking carbon microplates were retained upon surfactant modification. The high-magnification SEM image indicated no appreciable carbon depositing on the surface (Figure S2c). Since no appreciable microstructure changes could be observed in the SEM image, we conducted a N_2-BET analysis to probe changes in the RAC's microstructure.

3.2. Microstructure Analysis of Surfactant-Modified RAC

Figure 2a shows the N_2 adsorption–desorption isotherms of ref AC and modified RAC at 77 K. At the low relative pressure (P/P_0) end, the quantities of N_2 adsorbed by AC ref, surf 1, and surf 4 were comparable. The quantities of N_2 adsorbed by surf 2 and surf 5 were slightly higher, while that absorbed by surf 3 was the lowest. For the RAC modified using nonionic surfactants, the quantities of N_2 adsorbed by surf 6 and surf 8 were higher than that absorbed by AC ref, while surf 7 exhibited the lowest N_2 adsorption. Interestingly, all surfactant-modified RAC samples exhibited a well-defined plateau (relatively horizontal plateau) and hysteresis loop. In contrast, the quantity of N_2 adsorption by AC ref increased significantly with increasing P/P_0. In addition, the adsorption tail of AC ref at high P/P_0 was evident compared with that of surfactant-modified RAC. As micropores are preferentially filled at low P/P_0, the steep increase in the isotherm near the origin indicates the existence of a micropore-rich environment in the ref AC and surfactant-modified RAC [16]. Once the micropores and the mesopores with sizes of <4 nm were filled with adsorbed N_2, the adsorption isotherm reached a plateau, and the remaining mesopores were gradually filled in this stage. Accordingly, the changed isotherms shown in Figure 2a indicate that the microstructure of surfactant-modified RAC was distinctly different from that of ref AC. The disappearance of the adsorption tail at high P/P_0 further evidenced the reduction in macropores by surfactant modification. Along with the modified microstructure, changes in the pore volume occurred, as indicated in Figure 2a. Supporting our speculation, the porous AC ref was composed of a slightly higher $PV_{meso} + PV_{macro}$ than PV_{micro}. Importantly, surfactant modification considerably increased PV_{micro} while simultaneously reducing $PV_{meso} + PV_{macro}$. In this case, surfactant-modified RAC became micropore-rich by exhibiting much higher PV_{micro} than $PV_{meso} + PV_{macro}$. Consequently, their isotherm plateau appeared at a lower P/P_0 relative to AC ref. As illustrated in Figure 1, we speculated that the carbonized surfactant in the mesopores and macropores of AC accounted for the changes in the microstructure of the surfactant-modified RAC. This speculation was based on the results of the dissipative particle dynamics simulations regarding the concentration dependence of surfactant adsorption on small-diameter carbon nanotubes and their bundles [27]. In those simulations, the authors concluded that aggregation dominated adsorption on individual tubes, whereas it was largely a Langmuir-type process on bundles. This was because the strong van der Waal forces, along with solid hydrophobic interactions between individual tubes, made the surfaces of individual tubes inaccessible

for the surfactants. Accordingly, adsorption became progressively dominated by the total surface area of the bundle at a high surfactant concentration. We suspect that similar interfacial behaviors, the Langmuir-type process, would also happen on AC surfaces. In this configuration, surfactants were adsorbed at the AC's surface in a monolayer manner. Carbonized surfactants in the regeneration process transformed mesopores and macropores into abundant micropores. Significantly increased PV_{micro} accompanied by a reduction in $PV_{meso} + PV_{macro}$ was therefore observed.

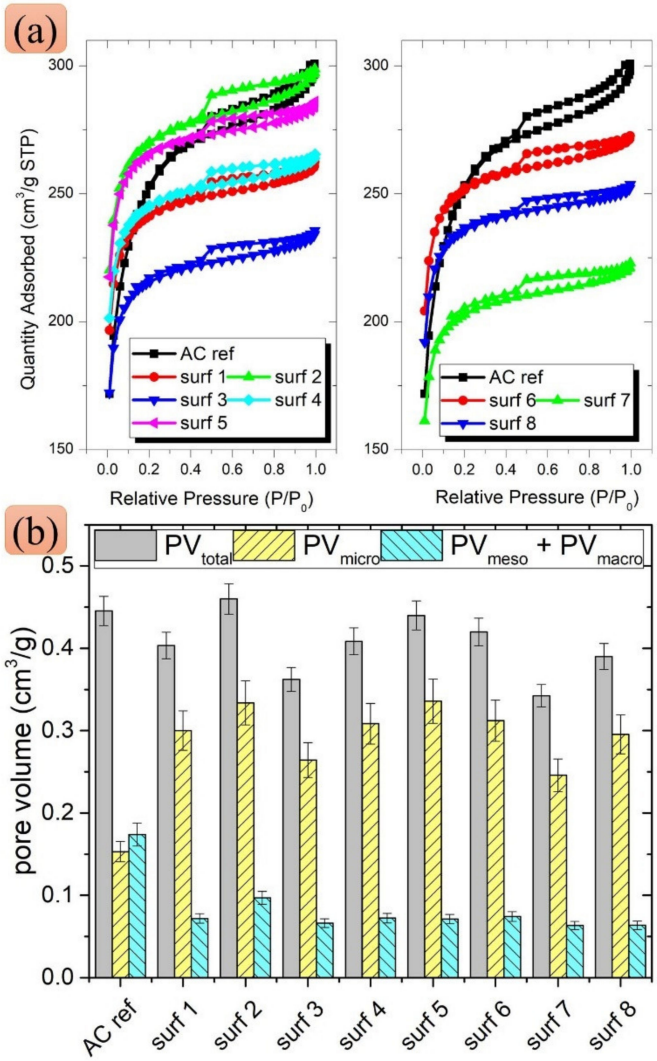

Figure 2. (**a**) N_2 adsorption–desorption isotherms at 77 K and (**b**) total pore volume (PV_{tot}), PV_{micro}, and $PV_{meso} + PV_{macro}$ of raw and surfactant-modified RAC.

To closely inspect the microstructure changes, the stack column plots of PV_{micro} and $PV_{meso} + PV_{macro}$ of ref AC and surfactant-modified RAC were arranged (Figure 3a). As shown in Figure 3a, the PV_{tot} of all surfactant-modified RACs was higher, or at least comparable, to that of AC ref, and all surfactant-modified RACs were full of micropores (~80%). This indicates that the surfactant modification successfully yielded micropore-rich RAC. More pore volume was not necessarily meant to increase the surface area, as shown in Figure 3b. For example, all surfactant-modified RACs exhibited a higher pore volume than the AC ref. However, only surf 2 and surf 5 had slightly higher surface areas than AC

ref. This is simply because the used adsorption model was different. The BET surface area (a_s, $m^2\ g^{-1}$) was estimated theoretically using Equation (1) [28]:

$$a_s = n_m a_m N_A \quad (1)$$

where n_m (mol-$N_2\ g^{-1}$) is the monolayer amount of adsorbed N_2, a_m is the molecular cross-sectional area (0.162 nm^2 is assigned for nitrogen at 77 K), and N_A is the Avogadro constant ($6 \times 10^{23}\ mol^{-1}$). The monolayer amount, n_m, was calculated using the BET Equation (2):

$$\frac{P/P_0}{n_a(1-P/P_0)} = \frac{1}{n_m C} + \frac{C-1}{n_m C}\frac{P}{P_0} \quad (2)$$

where n_a (mol g^{-1}) refers to the amount of N_2 adsorbed by measuring the difference in nitrogen pressure as a result of gas adsorption and the C value is an empirical BET constant that gives an indication of the order of magnitude of the attractive adsorbent–adsorbate interactions. The monolayer amount of gas adsorbed (n_m) and the C value were estimated from the slope and intercept by plotting the $\frac{P/P_0}{n_a(1-P/P_0)}$ against P/P_0 on the abscissa. In this configuration, the surface area (a_s) was calculated by assuming the surface area was occupied by the adsorbed gas in a complete monolayer manner. However, the reported micropore volume was determined via the t-plot method, which compares the shape of a given isotherm with that of a nonporous standard solid. $PV_{meso} + PV_{macro}$ was derived using the BJH method based on the macroscopic Kelvin equation [28]. Accordingly, some cases did not exhibit increased surface area accompanied by increased pore volume. Nonetheless, it is evident that surfactant modification indeed transformed PV_{meso} and PV_{macro} into abundant PV_{micro}.

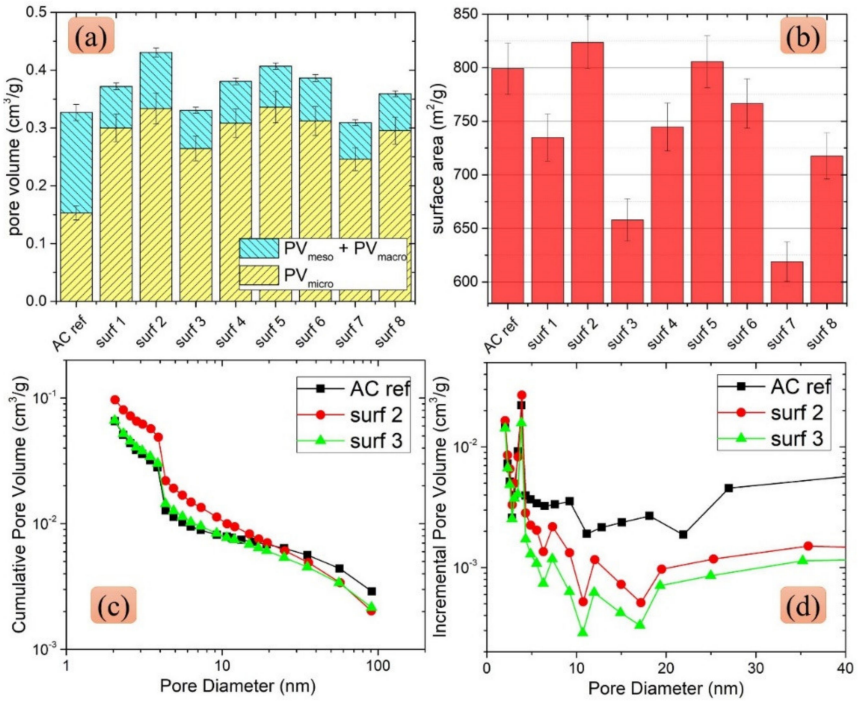

Figure 3. (**a**) Stack column plots of PV_{micro} and $PV_{meso} + PV_{macro}$ and (**b**) surface area of raw and surfactant-modified regenerated AC; representative (**c**) cumulative and (**d**) incremental pore volumes of the BJH desorption pore distributions of raw, surf 2, and surf 3 RAC.

Unfortunately, at this stage, we cannot establish a clear conclusion regarding which property would be the dominant factor that yielded the highest fraction of PV_{micro}. For example, the lengths of the hydrophobic tails of selected anionic surfactants did not significantly differ from those of one another. They all contained around 12–16 carbon/nitrogen

atoms in their hydrophobic tails. The difference in their molecular weight was also not significant. However, PV_{micro} was highest in surf 2 and surf 5, but lowest in surf 3. In the case of modification using nonionic surfactants, the hydrophilic head of surfactant 6 was the shortest, while that of surfactant 8 was the longest. However, surf 7 exhibited the least amount of PV_{micro} and the smallest surface area among them. The type of surfactant (anionic vs. nonionic), the molecular weight of the surfactant, and the length of their hydrophobic tail were not the decisive factors regulating the yield of the micropore volume. Furthermore, the concentrations of the eight surfactants were not equivalent due to different contents. The functional groups of the used surfactants also varied (Table 1). However, a general pattern was noted that surfactant modification substantially yielded a micropore-dominant RAC. This implies that the success of transforming meso-/macropores into micropores strongly relies on the association of surfactants in the meso-/macropores. In this case, reducing the surface tension of the AC is critical, as it allows carbon precursors to approach and reside in the pores of the AC. This phenomenon explains that the success in yielding abundant micropores is insensitive to the type of surfactants used. The surfactant-type-independent phenomenon further opens a new window for waste surfactant treatment, i.e., applying low-grade surfactants/surfactant cocktails to upgrade the RAC. Due to the cost of separation and purification of low-grade surfactants/surfactant mixtures, they are usually directly disposed of in industry. Our results demonstrate that the success in yielding abundant micropores is independent of the type of surfactants; they could be the raw materials for surfactant modification based on the circular economy concept.

The pore size distribution is another important property of porous materials. For example, hierarchical carbon with a desirable pore size distribution is beneficial for achieving the fast diffusion of electrolytes [29,30]. As mentioned above, hierarchical carbon is usually prepared via the pyrolysis of carbon sources, such as resin or polymers containing inorganic salts as hard templates [10,31]. To ease the environmental burden, green activation by potassium salt or Na/K mixture salt to concurrently serve as the salt template and high-energy molten salt media that can be operated without inert gas protection has been proposed [30,32]. Upgrading RAC to possess a desirable hierarchical structure would more straightforwardly respond to the perspective of the circular economy. The BJH desorption pore size distributions in terms of the cumulative pore volume of raw and surfactant-modified RAC are shown in Figure 3c. To avoid the complexity of the superimposed data, the representative cumulative pore volume curves of surf 2 and surf 3, which reflect the highest and lowest surface areas, were selected. As noted in Figure 3c, the shapes of the cumulative pore volume curves of surf 2 and surf 3 were, in general, unaffected by the surfactant modification. However, the curves shifted upward in the region with a pore size of <20 nm and bent downwards when the pore size exceeded 20 nm. This indicates that increased PV_{micro} was achieved by reducing $PV_{meso} + PV_{macro}$. A similar pattern was observed in the incremental pore volume curves shown in Figure 3d, in which the incremental pore volume of surf 2 and surf 3 considerably dropped when the pore size was >5 nm compared with that of the AC ref. This supports our speculation in Figure 1 that the carbonization of associated surfactants could effectively transform mesopores and macropores into abundant micropores. An important message implicated by the superimposed cumulative/incremental pore volume curves is that repartitioning the pore size distribution by surfactant modification is a universal pattern, not just a special case. Confirming that the repartition of the pore size distribution by modification is a universal pattern is very important from the perspective of the circular economy. This is because the best waste treatment is to equip the waste with additional functionalities to enable it to return to the market. On the other hand, the pore size distribution of surfactant-modified RAC is wider compared with that of synthesized carbon molecular sieves, metal–organic frameworks, and zeolites [33,34]. Furthermore, although the creation of a micropore usually generates a higher surface area, some modified RACs (such as surf 3 and surf 7) were noted to have more micropores, but low surface areas. We speculate that the inevitable experimental fluctuations along with uncertainty in evaluating the micropore volume from the isotherm

curve were likely responsible for the observation. However, it is certain that the surfactant modification, in general, led to the modified RAC having a higher micropore volume. It is worth mentioning that there are many effective methods to synthesize microporous AC with a high surface area, for example, applying activating agents, such as $ZnCl_2$ [11] and KOH [12]. The additional pre-carbonization process effectively yields a less-defective intermediate for developing abundant micropores in the subsequent activation step [35]. However, they might not be the best choice in response to the perspective of the circular economy for two reasons. First, acid washing is necessary to wash away abundant residue from chemical activation, and the treatment of acid effluent is thus an issue of concern [35]. Second, the waste AC is already full of micropores, so exploring an appropriate outlet for waste AC would be particularly interesting. Based on the above discussions, although the best surfactant modification (surf 3) only gave rise to about a 3% enhancement in the surface area relative to the original sample, our proposed surfactant modification would still be a promising solution for upgrading waste AC.

3.3. Microstructure Analysis of Gel Modified RAC

To prepare mesopore/macropore-rich RAC for fast ion transport [30], gel modification was conducted by dispersing AC in a gel containing a methyl cellulose thickening agent and surfactant. The methyl cellulose could behave as a binder bringing carbon plates/grains together in this gel system, while the surfactant could keep the gel fluid [36]. The carbonization of methyl cellulose and the surfactant matrix thus leaves additional mesoporous texture in the RAC. Indeed, the SEM image shown in Figure S3a reveals that carbonized methyl cellulose exhibited a coarse texture with a BET surface area as low as 0.33 $m^2\ g^{-1}$. In contrast, the carbonization of the matrix of methyl cellulose and surfactant produced a smooth surface (Figure S3b). The BET surface area of the carbonized matrix was increased to 16.62 $m^2\ g^{-1}$, indicating that the addition of surfactant not only homogenized the matrix (and thus resulted in a smooth surface), but also facilitated the development of a porous microstructure. Importantly, Figure S3a,b suggests that the extra surface area contributed by the gel matrix was very limited. We thus confidently attribute any observed changes in the microstructure of the gel-modified RAC to the modification itself. Representative low- (200×, Figure S3c) and high-magnification (2000×, Figure S3d) SEM images of gel 2 suggest that the surface of the obtained RAC was covered with randomly distributed rods and irregularly shaped fine particles. This means that a significant portion of the gel matrix might have been left at the AC surface. Supporting our speculation, the gel was mainly responsible for binding carbon particles together. Once carbonized, an interconnected mesoporous configuration could hence be developed.

Figure 4a shows the N_2 adsorption–desorption isotherms of the raw and gel-modified RAC at 77 K. Unlike surfactant modification, gel modification significantly reduced the surface area of RAC, as indicated by the downward-shifted isotherms. This indicates that gel modification considerably repartitioned micropores and mesopores [28,37]. As indicated in Figure 4b, both PV_{micro} and $PV_{meso} + PV_{macro}$ were reduced by gel modification. However, the amount of PV_{micro} and $PV_{meso} + PV_{macro}$ reduction was distinctly different and sensitive to the gel type applied. No conclusive pattern could be identified in this stage regarding which property of the gel would be the crucial factor governing the selectivity in PV_{micro} and $PV_{meso} + PV_{macro}$ reduction. However, it was noticed that most gel-modified RACs possessed higher $PV_{meso} + PV_{macro}$ than PV_{micro}, except for gel 1. Despite the decrease in the PV_{tot} of all gel-modified RAC to a certain extent, gel modification is generally capable of yielding mesopore-rich RAC.

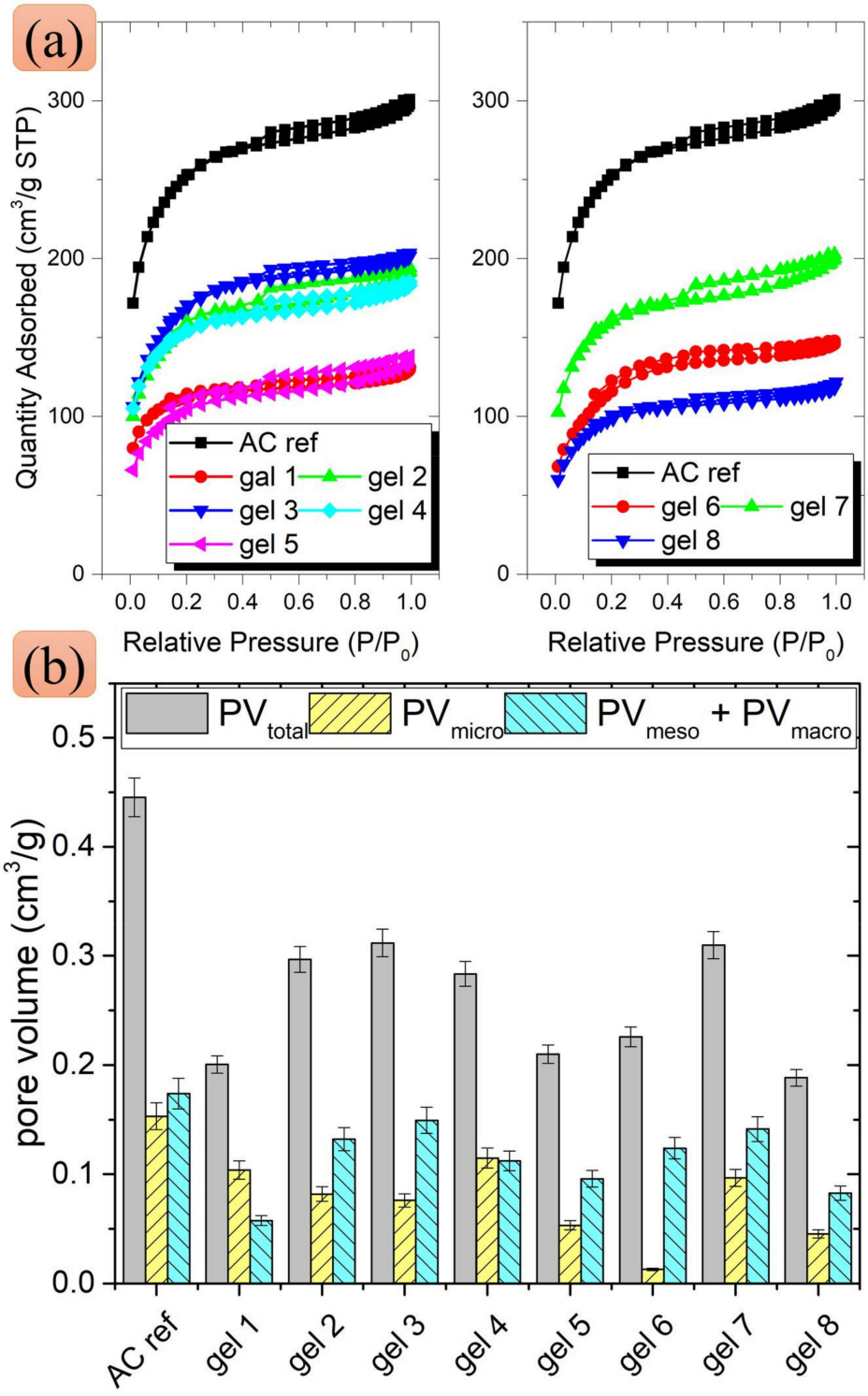

Figure 4. (**a**) N_2 adsorption–desorption isotherms at 77 K and (**b**) total pore volume (PV_{tot}), PV_{micro}, and $PV_{meso} + PV_{macro}$ of raw and gel-modified RAC.

Stack column plots of PV_{micro} and $PV_{meso} + PV_{macro}$ for the raw and gel-modified RAC are presented in Figure 5a. As indicated in Figure 5a, all gel-modified RACs had simultaneously decreased PV_{micro} and $PV_{meso} + PV_{macro}$ compared with ref AC. While gel 1 was relatively PV_{micro}-dominant and gel 6 showed an extremely high amount of $PV_{meso} + PV_{macro}$, the remaining gel-modified RAC contained a higher portion of $PV_{meso} + PV_{macro}$. Figure 5b shows the reducing surface area along with the changes in the fraction of $PV_{meso} + PV_{macro}$.

For the simplicity of the figure, the cumulative pore volume curves of gel 1 (relatively PV_{micro}-dominant) and gel 6 (extremely high amount of $PV_{meso} + PV_{macro}$) were selected and presented in Figure 5c. As shown in Figure 5c, gel modification bent the head (pore size <4 nm) of the curve of gel 1 upward, shifted the curve downward in the mesopore region slightly, and bent the tail of the curves downward in the macropore region. This led to the concurrently increased PV_{micro} and decreased $PV_{meso} + PV_{macro}$ of gel 1 (Figure 5d). Although the head of the cumulative pore volume curve of gel 6 was unaffected by the gel modification, the curve was vertically shifted upward in the mesopore region, and the tail was bent downward in the macropore region (Figure 5c). This corresponded to decreases of ~ 90% and ~30%, respectively, in PV_{micro} and $PV_{meso} + PV_{macro}$ of gel 6 relative to those of AC ref. Accordingly, gel 6 possessed an extremely high amount of $PV_{meso} + PV_{macro}$ due to gel modification. Importantly, Figure 5b further reveals that the loss in surface area was the inevitable trade-off in gel modification to yield mesoporous RAC. Despite this inevitable trade-off, gel modification would likely be, to the best of our knowledge, the most cost-effective method to upgrade waste AC by exhibiting a mesoporous structure for high-end applications. For example, increased pore width of a carbon material could improve the selectivity in separating large ions, such as Ca(II), from high-concentration Na(I) solutions [4].

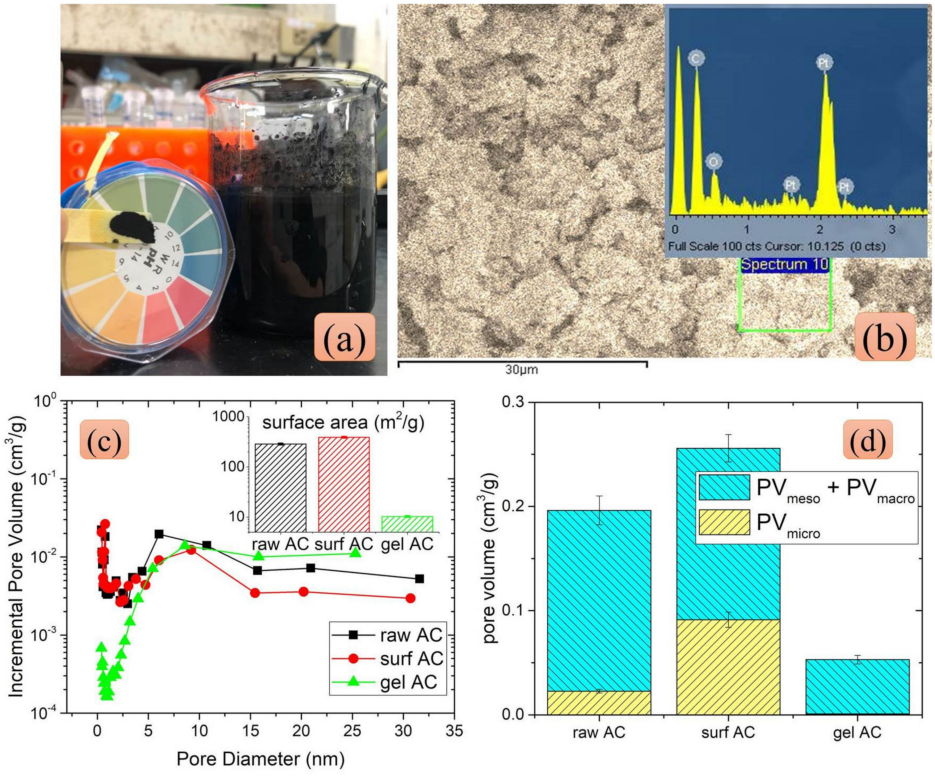

Figure 5. (**a**) Stack column plots of PV_{micro} and $PV_{meso} + PV_{macro}$ and (**b**) surface area of raw and gel-modified regenerated AC; representative (**c**) cumulative and (**d**) incremental pore volumes of the BJH desorption pore distributions of the raw, gel 1, gel 3, and gel 6 RACs.

3.4. Validity of Real Waste AC Samples

Conducting a life-cycle assessment would determine the contribution of upgrading waste AC, i.e., sending upgraded AC back to the market, to reducing a certain amount of carbon emissions from landfilling/incinerating waste AC. However, the detailed environmental impact of releasing the environmental burden through upgrading waste AC and sending them back to the market is unclear. To demonstrate the potential of our proposed upgrade methods, we alternatively conducted additional electrochemical experiments using waste AC powders as the model material. The waste AC powders (referred to as

raw AC) were collected from the sewage sludge of CACI. As shown in Figure 6a, they were disintegrated fine AC particles with particle sizes of around several micrometers. The pH of the raw AC sewage sludge was around pH 6–7. Considering the difficulty in the separation and purification, they are usually directly disposed of, despite their high carbon content (indicated by the EDX analysis, provided in Figure 6b). Upgrading these waste AC powders is, therefore, important from the perspective of the circular economy. We applied the identical modification protocol to modify the raw AC using surfactant 6 (surf AC) and the gel containing the mixture of surfactant 6 and methyl cellulose (gel AC). As shown in Figure 6c, surfactant modification clearly increased the surface area of surf AC relative to that of the raw AC. From the pore size distribution profile, increased surface area was achieved by transforming mesopores into micropores. In contrast, gel modification profoundly reduced the surface area of the gel AC due to the disappearance of PV_{micro}. This substantially supports our proposed concept that gel modification could effectively yield mesoporous RAC (Figure 6d). Either way, by the surfactant/gel modification, the as-obtained RAC would exhibit different surface properties that allow for new applications.

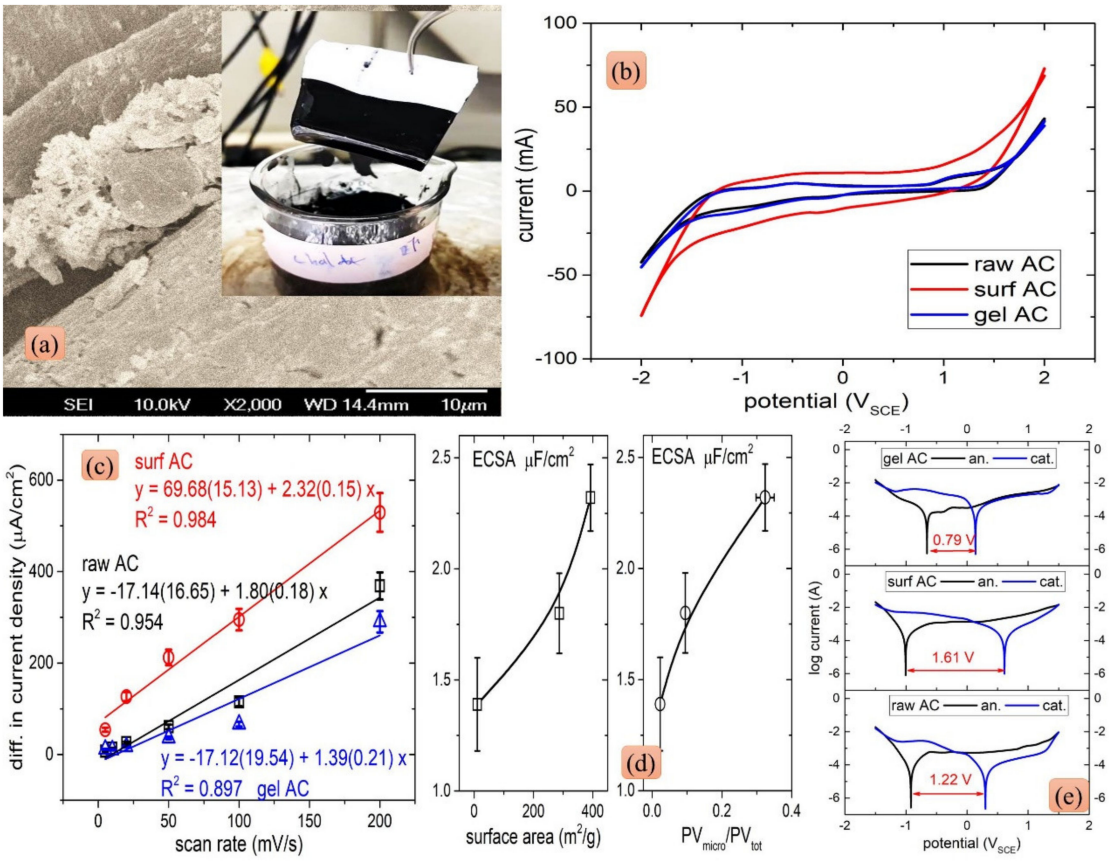

Figure 6. (**a**) SEM image of the as-obtained gel AC electrode, insert: photograph of the dipping process in electrode preparation; (**b**) CV scans of the as-obtained raw, surf, and gel AC electrodes; (**c**) difference in the anodic/cathodic capacitive currents ($\Delta J = Ja - Jc$) at 0.10 V_{SCE} against the scan rate. The slopes were obtained by linear regression; (**d**) correlation between the determined ECSA and the surface area (left) and PV_{micro}/PV_{tot} (right); (**e**) Tafel plots of the as-obtained raw, surf, and gel AC electrodes.

Unlike the surf AC, the economic value of the gel-modified RAC that had a lower surface area and smaller meso/macropore volume might be subtle. Given that the meso/macropores were the fast channels for ion transport [30], we hence fabricated electrodes with these RACs to demonstrate the unique role of meso/macropores in electrochemical applications. The electrodes were fabricated by dipping the 2 cm × 3 cm Ti mesh in 100 mL

methylpyrrolidone slurry containing 10 mg RAC, 80 mg carbon black, and 10 mg polytetrafluoroethylene [24]. They were dried at 90 °C overnight and the mass loadings of these electrodes were about 2 mg cm^{-2} (inserted Figure 6a). As observed in the SEM image (Figure 6a), associated RACs were well-dispersed over the Ti mesh. It must be mentioned that the objective of the conducted electrochemical analyses was to signify the unique role of meso/macropores in electrochemical behaviors. The optimization of the performance was hence not conducted. A series of cyclic voltammetry (CV) scans using symmetry electrodes (both the working and counter electrodes were the same) were conducted in 10 mM NaCl at pH 6.8 ± 0.2. As shown in Figure 6b, the surf AC had the largest area, while the gel AC exhibited the lowest area under the CV curves. This indicates the important role of micropores in developing electric double layer (EDL) capacitance [38]. As the gel AC contained very limited micropores, the lowest EDL capacitance was thus observed. In addition to developing EDL capacitance, the electrochemically active surface area (ECSA) could be further evaluated from these CV curves by plotting the difference in the anodic/cathodic capacitive current (ΔJ = Ja − Jc) at 0.10 V_{SCE} against the scan rate. The slope, which was twice the EDL capacitance, could be obtained by the linear regression representing the corresponding ECSA in this configuration [31]. As shown in Figure 6c, the slopes of the raw AC, surf AC, and gel AC were 1.80 ± 0.18, 2.32 ± 0.15, and 1.39 ± 0.21 μF cm^{-2}, respectively. As suggested by the spline line included in Figure 6d, the increment in ECSA increased significantly with increasing surface area. By plotting the determined ECSA against the PV_{micro}/PV_{tot}, it is interesting to note that the increment in ECSA did not proportionally increase with increasing PV_{micro}/PV_{tot}. This emphasizes the meso/macropores' unique role in providing a fast channel for ion transport [39]. That is, ECSA could be regarded as having an effective surface area accessible to ions. Although the ECSA could also be influenced by the possible N-/S-doping and introduced functional groups due to the modification (the used surfactants bear N-/S-functional groups, Table 1, Figure S1), it appears that the microstructure had a more profound impact on the observed ECSA. The Tafel slope could further emphasize the significance of a fast channel for ion transport [40,41]. As indicated by the differences in the overpotentials derived from the anodic (an.) and cathodic (cat.) branches of the CV scan (±1.5 V^{SCE}, 100 mV s^{-1}), the gel AC had the lowest difference in terms of the overpotential (Figure 6e). It is interesting to note that, despite the modified RAC only accounting for one-tenth of the mass loading, the determined difference in the overpotential of gel AC could be reduced by ~35% compared with that of the raw AC. In contrast, the difference in the overpotential could be increased by ~30% in the micropore-rich surf AC. This again emphasizes the importance of pore size in the electrochemical application of carbonaceous materials. For example, the formation of highly mesoporous solids favors the diffusion of CO_2 molecules into the material; thus a high CO_2 separation efficiency could be reached [42]. Micropore-rich biochar exhibits high efficiency in selectively removing hardness-causing cations, such as calcium and magnesium [43]. Although we cannot precisely tune the pore size of the modified RAC yet, our proposed modification method is definitely capable of affording the modified RAC new properties for electrochemical applications.

4. Conclusions

The regenerated activated carbon (RAC) could exhibit new surface properties by manipulating its microstructures that give rise to additional RAC applications based on the spirit of the circular economy. This was achieved by carbonizing associated carbon precursors, such as commercially available low-cost surfactants and the gel-containing surfactant and methyl cellulose thickening agent in the pores of AC. The RAC obtained through surfactant and gel modification would be micropore-predominant and meso-/macropore-rich, respectively. The meso-/macropores could be effectively transformed in this configuration by carbonized surfactants, leading to the production of micropore-rich RAC. In contrast, the carbonized gel would block micropores and thus give rise to meso-/macroporous RAC. Notably, the microstructure adjustment by surfactant/gel

modification was a universal pattern, not just a special case. This universal pattern indicates the promising potential of surfactant/gel modification in waste treatment. Although the loss in surface area was the inevitable trade-off in some cases, the RAC could be upgraded by possessing new, interesting microstructures for some high-end applications. Our result offers an important demonstration from the perspective of the circular economy.

Supplementary Materials: The following supporting information can be downloaded at: https://www.mdpi.com/article/10.3390/pr10081631/s1, Figure S1: Representative (a) XRD; FTIR spectra of (b) raw and surfactant-modified RAC, and (c) surfactant 1 and surfactant 6; Figure S2: (a) Representative size distribution of surfactant 1 solution (diluted by 10 times and in the final 1 min of measurement) determined by dynamic light scattering; and the (b) low- (200×) and (c) high-magnification (2000×) SEM images of surf 1 sample; Figure S3: Representative SEM images of carbonized (a) methyl cellulose and (b) matrix of methyl cellulose and surfactant 2, and (c) low- (200×) and (d) high-magnification (2000×) images of gel 2.

Author Contributions: Conceptualization, T.-H.W. and C.-D.D.; methodology, T.-H.W. and C.-W.C.; formal analysis, T.-H.W. and C.-C.C.; investigation, C.-C.C. and R.-X.X.; data curation, T.-H.W.; C.-C.C. and R.-X.X.; writing—original draft preparation, T.-H.W. and C.-W.C.; writing—review and editing, T.-H.W., C.-W.C. and C.-D.D. All authors have read and agreed to the published version of the manuscript.

Funding: This research acknowledges the financial support from the Ministry of Science and Technology, Taiwan, MOST 109-2221-E-155-010-MY3; MOST 111-2221-E-155-011. The authors gratefully acknowledge the access to the Instrument Center of National Tsing Hua University for characterization instrumentation.

Institutional Review Board Statement: Not applicable.

Informed Consent Statement: Not applicable.

Data Availability Statement: The data presented in this study are available on request from the corresponding authors.

Conflicts of Interest: The authors declare no conflict of interest. The funders had no role in the design of the study; in the collection, analyses, or interpretation of data; in the writing of the manuscript; or in the decision to publish the results.

References

1. Hu, G.P.; Zhao, Q.H.; Tao, L.F.; Xiao, P.; Webley, P.A.; Li, K.G. Enrichment of low grade CH_4 from N_2/CH_4 mixtures using vacuum swing adsorption with activated carbon. *Chem. Eng. Sci.* **2021**, *229*, 116152. [CrossRef]
2. Wang, T.H.; Yang, C.C.; Qin, K.; Chen, C.W.; Dong, C.D. Life time enhanced Fenton-like catalyst by dispersing iron oxides in activated carbon: Preparation and reactivation through carbothermal reaction. *J. Hazard. Mater.* **2021**, *406*, 124791. [CrossRef] [PubMed]
3. Ganash, A.A.; Alghamdi, R.A. Fabrication of a novel polyaniline/green-synthesized, silver-nanoparticle-modified carbon paste electrode for electrochemical sensing of lead ions. *J. Chin. Chem. Soc.* **2021**, *68*, 2312–2325. [CrossRef]
4. Ceron, M.R.; Aydin, F.; Hawks, S.A.; Oyarzun, D.I.; Loeb, C.K.; Deinhart, A.; Zhan, C.; Pham, T.A.; Stadermann, M.; Campbell, P.G. Cation Selectivity in capacitive deionization: Elucidating the role of pore size, electrode potential, and ion dehydration. *ACS Appl. Mater. Interfaces* **2020**, *12*, 42644–42652. [CrossRef]
5. Chen, S.K.; Chang, K.H.; Hsu, C.H.; Lim, Z.Y.; Du, F.Y.; Chang, K.W.; Chang, M.C.; Lin, H.P.; Hu, C.C.; Tang, C.Y.; et al. Synthesis of mesoporous carbon platelets of high surface area and large porosity from polymer blends-calcium phosphate nanocomposites for high-power supercapacitor. *J. Chin. Chem. Soc.* **2021**, *68*, 462–468. [CrossRef]
6. Sanyal, O.; Hicks, S.T.; Bhuwania, N.; Hays, S.; Kamath, M.G.; Karwa, S.; Swaidan, R.; Koros, W.J. Cause and effects of hyperskin features on carbon molecular sieve (CMS) membranes. *J. Membr. Sci.* **2018**, *551*, 113–122. [CrossRef]
7. Wu, S.J.; Yan, P.J.; Yang, W.; Zhou, J.; Wang, H.; Che, L.; Zhu, P.F. $ZnCl_2$ enabled synthesis of activated carbons from ion-exchange resin for efficient removal of Cu^{2+} ions from water via capacitive deionization. *Chemosphere* **2021**, *264*, 128557. [CrossRef]
8. Li, S.S.; Chen, Q.Y.; Gong, Y.N.; Wang, H.; Li, D.L.; Zhang, Y.P.; Fu, Q.; Pan, C.X. "One-Step" carbonization activation of garlic seeds for honeycomb-like hierarchical porous carbon and its high supercapacitor properties. *ACS Omega* **2020**, *5*, 29913–29921. [CrossRef]
9. Ai, J.G.; Yang, S.H.; Sun, Y.N.; Liu, M.; Zhang, L.; Zhao, D.G.; Wang, J.Q.; Yang, C.; Wang, X.T.; Cao, B.Q. Corncob cellulose-derived hierarchical porous carbon for high performance supercapacitors. *J. Power Sources* **2021**, *484*, 229221. [CrossRef]

10. Yi, Y.J.; Hou, Y.; Li, Y.M. Preparation of high conductivity hierarchical porous carbon based on sodium lignosulfonate with pre-crosslinking. *Bioresources* **2020**, *15*, 8995–9012. [CrossRef]
11. Van Veenhuyzen, B.; Tichapondwa, S.; Horstmann, C.; Chirwa, E.; Brink, H.G. High capacity Pb(II) adsorption characteristics onto raw- and chemically activated waste activated sludge. *J. Hazard. Mater.* **2021**, *416*, 125943. [CrossRef]
12. Gyu, H.O.; Chong, R.P. Preparation and characteristics of rice-straw-based porous carbons with high adsorption capacity. *Fuel* **2002**, *81*, 327–336.
13. Ntakirutimana, S.; Tan, W. Synergistic effects of ionic and nonionic surfactants treatment on activated carbon electrodes for inverted capacitive deionization. *Sep. Purif. Technol.* **2021**, *258*, 117987. [CrossRef]
14. Mukerjee, P.; Mysels, K.J. *Critical Micelle Concentration of Aqueous Surfactant Systems*; NSRDS-NBS 36; U.S. Government Printing Office: Washington, DC, USA, 1971.
15. Sizirici, B.; Fseha, Y.H.; Yildiz, I.; Delclos, T.; Khaleel, A. The effect of pyrolysis temperature and feedstock on date palm waste derived biochar to remove single and multi-metals in aqueous solutions. *Sustain. Environ. Res.* **2021**, *31*, 9. [CrossRef]
16. *ISO 9277:2010*; Determination of the Specific Surface Area of Solids by Gas Adsorption—BET Method. 2nd ed. ISO: London, UK, 2010.
17. Suganuma, S.; Nakajima, K.; Kitano, M.; Yamaguchi, D.; Kato, H.; Hayashi, S.; Hara, M. Hydrolysis of cellulose by amorphous carbon bearing SO_3H, COOH, and OH groups. *J. Am. Chem. Soc.* **2008**, *130*, 12787–12793. [CrossRef]
18. Sun, Z.X.; Zheng, M.T.; Hu, H.; Dong, H.W.; Liang, Y.R.; Xiao, Y.; Lei, B.F.; Liu, Y.L. From biomass wastes to vertically aligned graphene nanosheet arrays: A catalyst-free synthetic strategy towards high-quality graphene for electrochemical energy storage. *Chem. Eng. J.* **2018**, *336*, 550–561. [CrossRef]
19. Chen, H.; Wang, S.Q.; Zhang, X.M.; Zhao, Y.G.; Zhang, H. A study of chemical structural evolution of thermally altered coal and its effect on graphitization. *Fuel* **2021**, *283*, 119295. [CrossRef]
20. He, S.; Xu, Y.K.; Zhang, Y.S.; Bell, S.; Wu, C.F. Waste plastics recycling for producing high-value carbon nanotubes: Investigation of the influence of manganese content in Fe-based catalysts. *J. Hazard. Mater.* **2021**, *402*, 123726. [CrossRef]
21. Yuan, G.; Guan, K.X.; Hu, H.; Lei, B.F.; Xiao, Y.; Dong, H.W.; Liang, Y.R.; Liu, Y.L.; Zheng, M.T. Calcium-chloride-assisted approach towards green and sustainable synthesis of hierarchical porous carbon microspheres for high-performance supercapacitive energy storage. *J. Colloid Interface Sci.* **2021**, *582*, 159–166. [CrossRef]
22. Sevilla, M.; Ferrero, G.A.; Fuertes, A.B. One-pot synthesis of biomass-based hierarchical porous carbons with a large porosity development. *Chem. Mater.* **2017**, *29*, 6900–6907. [CrossRef]
23. Yea, D.; Lee, S.; Jo, S.; Yu, H.; Lim, J. Preparation of environmentally friendly amino acid-based anionic surfactants and characterization of their interfacial properties for detergent products formulation. *J. Surfactants Deterg.* **2018**, *21*, 541–552. [CrossRef]
24. Yang, J.W.; Tan, Z.X.; Chen, X.; Liang, Y.R.; Zheng, M.T.; Hu, H.; Dong, H.W.; Liu, X.R.; Liu, Y.L.; Xiao, Y. A mild method to prepare nitrogen-rich interlaced porous carbon nanosheets for high-performance supercapacitors. *J. Colloid Interface Sci.* **2021**, *599*, 381–389. [CrossRef] [PubMed]
25. Zhong, Y.; Deng, Q.; Yao, Q.; Lu, C.X.; Zhang, P.X.; Li, H.; Wang, J.; Zeng, Z.L.; Zou, J.J.; Deng, S.G. Functionalized biochar with superacidity and hydrophobicity as a highly efficient catalyst in the synthesis of renewable high-density fuels. *ACS Sustain. Chem. Eng.* **2020**, *8*, 7785–7794. [CrossRef]
26. Bueno, V.; Ghoshal, S. Self-assembled surfactant-templated synthesis of porous hollow silica nanoparticles: Mechanism of formation and feasibility of post-synthesis nanoencapsulation. *Langmuir* **2020**, *36*, 14633–14643. [CrossRef] [PubMed]
27. Angelikopoulos, P.; Bock, H. The differences in surfactant adsorption on carbon nanotubes and their bundles. *Langmuir* **2010**, *26*, 899–907. [CrossRef] [PubMed]
28. Sing, K.S.W.; Everett, D.H.; Haul, R.A.W.; Mouscou, L.; Pierotti, R.A.; Rouquerol, J.; Siemieniewska, T. Reporting physisorption data for gas/solid systems with special reference to the determination of surface area and porosity (Recommendations 1984). *Pure Appl. Chem.* **1985**, *57*, 603–619. [CrossRef]
29. Talreja, N.; Jung, S.; Yen, T.H.; Kim, T.Y. Phenol-formaldehyde-resin-based activated carbons with controlled pore size distribution for high-performance supercapacitors. *Chem. Eng. J.* **2020**, *379*, 122332. [CrossRef]
30. Wang, C.J.; Wu, D.P.; Wang, H.J.; Gao, Z.Y.; Xu, F.; Jiang, K. Biomass derived nitrogen-doped hierarchical porous carbon sheets for supercapacitors with high performance. *J. Colloid Interface Sci.* **2018**, *523*, 133–143. [CrossRef]
31. Xu, S.; Lin, C.; Wang, T.H.; Wang, C.F.; Chen, C.W.; Dong, C.D. Selective converting surface states of hematite photoelectrodes to catalytic active sites. *J. Chin. Chem. Soc.* **2021**, *68*, 1020–1029. [CrossRef]
32. Wang, C.J.; Wu, D.P.; Wang, H.J.; Gao, Z.Y.; Xu, F.; Jiang, K. A green and scalable route to yield porous carbon sheets from biomass for supercapacitors with high capacity. *J. Mater. Chem. A* **2018**, *6*, 1244–1254. [CrossRef]
33. Lawal, S.O.; Yu, L.; Nagasawa, H.; Tsuru, T.; Kanezashi, M. A carbon-silica-zirconia ceramic membrane with CO_2 flow-switching behaviour promising versatile high-temperature H_2/CO_2 separation. *J. Mater. Chem. A* **2020**, *8*, 23563–23573. [CrossRef]
34. Lei, L.F.; Bai, L.; Lindbrathen, A.; Pan, F.J.; Zhang, X.P.; He, X.Z. Carbon membranes for CO_2 removal: Status and perspectives from materials to processes. *Chem. Eng. J.* **2020**, *401*, 126084. [CrossRef]
35. Yun, C.H.; Park, Y.H.; Park, C.R. Effects of pre-carbonization on porosity development of activated carbons from rice straw. *Carbon* **2001**, *39*, 559–567. [CrossRef]

36. Klinthong, W.; Huang, C.H.; Tan, C.S. One-pot synthesis and pelletizing of polyethylenimine-containing mesoporous silica powders for CO_2 capture. *Ind. Eng. Chem. Res.* **2006**, *55*, 6481–6491. [CrossRef]
37. Thommes, M. Physical adsorption characterization of nanoporous materials. *Chem. Ing. Tech.* **2010**, *82*, 1059–1073. [CrossRef]
38. Xu, S.; Li, S.P.; Wang, T.H.; Wang, C.F. Effect of surface ionization of doped MnO_2 on capacitive deionization efficiency. *Langmuir* **2019**, *35*, 628–640. [CrossRef]
39. Largeot, C.; Portet, C.; Chmiola, J.; Taberna, P.L.; Gogotsi, Y.; Simon, P. Relation between the ion size and pore size for an electric double-layer capacitor. *J. Am. Chem. Soc.* **2008**, *130*, 2730–2731. [CrossRef]
40. Fan, K.; Chen, H.; Ji, Y.F.; Huang, H.; Claesson, P.M.; Daniel, Q.; Philippe, B.; Rensmo, H.; Li, F.S.; Luo, Y.; et al. Nickel–vanadium monolayer double hydroxide for efficient electrochemical water oxidation. *Nat. Comm.* **2016**, *7*, 11981. [CrossRef]
41. Fei, H.F.; Long, Y.D.; Yu, H.J.; Yavitt, B.M.; Fan, W.; Ribbe, A.; Watkins, J.J. Bimodal mesoporous carbon spheres with small and ultra-large pores fabricated using amphiphilic brush block copolymer micelle templates. *ACS Appl. Mater. Interfaces* **2020**, *12*, 57322–57329. [CrossRef]
42. Miricioiu, M.G.; Zaharioiu, A.; Oancea, S.; Bucura, F.; Raboaca, M.S.; Filote, C.; Ionete, R.E.; Niculescu, V.C.; Constantinescu, M. Sewage sludge derived materials for CO_2 adsorption. *Appl. Sci.* **2021**, *11*, 7139. [CrossRef]
43. Sepehr, M.N.; Zarrabi, M.; Kazemian, H.; Amrane, A.; Yaghmaian, K.; Ghaffari, H.R. Removal of hardness agents, calcium and magnesium, by natural and alkaline modified pumice stones in single and binary systems. *Appl. Surf. Sci.* **2013**, *274*, 295–305. [CrossRef]